Article

Kinetic Modeling of the Devolatilization of Pulverized Coal, Poplar Wood, and Their Blends in a Thermogravimetric Analyzer and a Flat Flame Reactor

Romain Lemaire,* Wei Wang, and Sebastien Menanteau
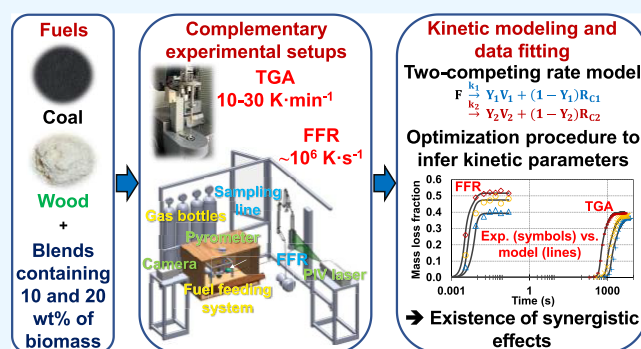
Cite This: *ACS Omega* 2023, 8, 29455−29467

Read Online

ACCESS | Metrics & More | Article Recommendations

ABSTRACT: Devolatilization kinetics of coal, poplar wood, and blends containing 10 and 20 wt % of biomass were characterized. Measurements were carried out under inert atmosphere with heating rates between 10 K min^{-1} and ~10^6 K s^{-1} using a thermogravimetric analyzer (TGA) and a flat flame reactor (FFR). Measured data were simulated using the chemical percolation devolatilization (CPD) model and a global kinetic scheme based on two competitive reactions integrating a refined differential reaction model. The CPD model failed to simulate TGA results but reproduced FFR data relatively well. As for the global model, selecting kinetic parameters from the literature turned out to lead to unsuitable predictions. Fitted values of the activation energies $E_{a,i}$, pre-exponential factors A_i, mass stoichiometric coefficients Y_i,

and the reaction model factor n were therefore inferred using a genetic algorithm-based optimization procedure, leading to obtain an excellent agreement between simulated and measured data. The assessed $E_{a,i}$ values were found to be lower for wood than for coal, which is consistent with the higher energy required to break the strong C−C bonds holding the highly cross-linked aromatic structures of coal. Besides, blending coal with 20 wt % of wood induced a decrease of $E_{a,i}$ values, which went from 99.79 to 86.1 kJ mol^{-1} and from 186.72 to 171.57 kJ mol^{-1} for the first and second reactions prevailing at low and high temperatures, respectively. Finally, the fact that the activation energy of the first devolatilization reaction was found to be lower with the blend containing 20% of wood than for wood illustrated the probable existence of synergies, as also exemplified by the characteristic devolatilization times for blended samples, which were found to be relatively similar to and even lower than that of wood.

1. INTRODUCTION

Demand for energy keeps increasing due to economic growth, and therefore, energy carriers such as coal will continue to play a key role in the coming decades, especially in Asian countries,[1] despite the major concerns regarding global warming. In an attempt to tackle even more stringent regulations aimed at limiting CO$_2$ emissions, considerable work still needs to be done to develop and/or improve the efficiency of current thermochemical conversion processes (e.g., combustion, pyrolysis, or gasification, as reviewed in ref 2, among others), which allow converting fossil fuels, renewable resources, or wastes into heat, electricity, and chemicals. Within this context, the co-combustion of coal with woody biomass (a carbon-neutral fuel) has attracted growing attention.[3−8] Cofiring indeed represents an interesting route to gradually decrease the consumption of fossil fuels, mitigate net greenhouse gas emissions, and extend the operating life of existing coal-based power plants, with reasonable retrofitting costs.[6−8] In expanding the application of co-combustion, a key challenge is to develop the computational codes required to

design and/or optimize the functioning of boilers operating with coal/biomass blends. Doing so implies gaining a fundamental knowledge of the mechanisms underlying the conversion of solid fuels in the conditions typically encountered in industrial facilities. Such complex thermochemical processes comprise successive steps, including devolatilization, which is highly critical as it initiates fuel thermal degradation in most industrial applications such as pulverized fuel boilers, gasifiers, carbonizers, and so forth. It thus directly impacts fuel conversion rates and kinetics as well as the nature and distribution of emitted products (i.e., char, tar, and gas). Furthermore, properly apprehending the devolatilization behavior of blends made up of coal and wood is all the

more critical since different works have reported more or less significant synergistic effects likely to promote the yields of volatiles emitted when both feedstocks are co-processed (see ref 9 and references therein). All these observations explain why, for more than five decades, particular attention has been devoted to the formulation of global and network models allowing to simulate the devolatilization behavior of different feedstocks, including coal and biomass (see refs 10−16 and references therein).

Apart from the reference isoconversional method,[17] which is commonly used to predict kinetic parameters based on the processing of thermogravimetric measurements,[12−14] the main models implemented to simulate devolatilization can be roughly classified into two categories. A distinction can indeed be made between global (or empirical) and network (or phenomenological) models, depending on whether they aim at simulating the rate of mass loss of the fuel and/or the distribution of pyrolytic products. As for global kinetic models, they include one-step,[18] two-competing rate,[19] and distributed activation energy (DAE)[20] approaches, which account for the devolatilization phenomenon by means of one, two, and an infinity of first-order reactions, respectively. Among the most used phenomenological models, one can cite the functional group−devolatilization-vaporization-cross-linking (FG-DVC),[21] the chemical percolation devolatilization (CPD),[22] and the flashchain[23] models. These comprehensive simulation tools consider the detailed structure changes undergone by thermally treated fuels through multiple mechanisms comprising depolymerization, vaporization, cross-linking, bridge-breaking and rearranging, side-chain cracking, and so forth. Although initially developed for coal, the different models listed above have been adapted and extensively used to simulate biomass devolatilization.[12−14,16] This is notably the case for the above network models for which specific versions have been proposed (e.g., Bio-FG-DVC,[24] Bio-CPD,[25] and Bio-flashchain[26]).

Major progress has thus been achieved in the modeling of the devolatilization kinetics. The predictive ability of global and network models still needs to be further validated and improved, however. These simulation tools indeed cannot fully capture the complexity and heterogeneity of coal and wood, whose decomposition is significantly influenced by numerous operating factors, including the temperature range and heating rate (HR). Phenomenological models which integrate such parameters to some extent have proven to provide relatively accurate predictions, as exemplified in the case of the CPD code.[27] Their intrinsic complexity, however, partly prevents them from being used for the simulation of full-scale boilers and gasifiers.[28] Continuous effort is therefore ongoing to evaluate and develop simpler global kinetic models,[28,29] even though their parametrization against trusted data prompts the need for additional experimental investigations conducted under widely varying thermal conditions.

As for the study of devolatilization at the laboratory scale, thermogravimetric analysis (TGA) remains the most implemented non-isothermal measurement approach.[9,11,12,14,16] It allows increasing the temperature of the tested sample with a constant heating rate while measuring the mass of the residual solid. Although this technique allows obtaining accurate mass loss curves with a high time resolution, only low heating rates (typically less than 50 K min^{-1}) can be set, which is significantly different from the conditions involved in industrial combustors. To tackle this issue, more realistic experimental

devices, including flat flame reactors (FFR)[30−32] and drop tube furnaces (DTF),[18,19,29,33] are also used. Fast heating rates between 10^4 and 10^6 K s^{-1} can then be reached, which allows the assessment of kinetic parameters that are more relevant for industrial applications. The characterization of the thermal history of the fuel in FFR and DTF is, however, far more difficult than during TGA experiments. It indeed requires implementing sophisticated diagnostics[31,32] and/or solving theoretical energy balances,[29,33] thus explaining why simpler thermogravimetric analyses are often preferred. Nevertheless, since the fuel heating rate directly influences the devolatilization process, as mentioned above, kinetic data derived from slow heating rate TGA measurements are not applicable to conditions associated with fast heating devices, and vice versa.[16] This has been exemplified in numerous works which show that the fractions of volatile matters emitted during high HR tests can reach values much higher than their counterparts issued from thermogravimetric or proximate analyses.[19,29,32] Deriving kinetic parameters suitable for simulating the devolatilization behavior of solid fuels such as coal or wood over an extended range of thermal conditions, therefore, implies parametrizing global modeling tools based on comprehensive sets of data, combining both low and high HR measurements.[29]

Within this context, the present work aims at experimentally characterizing and modeling the devolatilization behavior of fuels of specific interest for cofiring and co-pyrolysis applications (i.e., high volatile bituminous coal, poplar wood, and their blends). The pyrolysis of coal and wood blends has been recently studied in ref 34. This preliminary analysis, however, solely focused on low heating rate measurements (<30 K min^{-1}), noting that obtained data were modeled using basic isoconversional approaches. In the present work, new measurements were carried out with similar samples but using two complementary analytical devices (TGA and FFR) in order to assess devolatilization profiles, with HR comprised between 10 K min^{-1} (TGA) and ∼10^6 K s^{-1} (FFR). To the best of the authors' knowledge, modeling studies of coal/biomass devolatilization conducted based on data acquired by coupling TGA and FFR are relatively rare (if at all existing), which thus represents an original feature of this study. Obtained data were simulated by means of a reference network model (i.e., the CPD) and a two-competing rate scheme integrating a refined differential reaction model proposed by Authier et al.[29] Proceeding as such allowed the comparison of the predictive ability of both these widely implemented, albeit quite different, modeling approaches. Furthermore, and according to ref 29, the selection and parametrization of a two-competing rate model is particularly relevant due to the overall simplicity of such an approach which can be implemented easily and numerically solved in the devolatilization sub-models of commonly used CFD softwares. Regarding the calculations achieved with the two-step model, different sets of kinetic parameters from the literature were first tested. Optimized constants were then inferred by means of a fitting procedure involving a genetic algorithm-based optimizer. Obtained results were finally analyzed to characterize the devolatilization behavior of the tested fuels as well as the possible synergies encompassing the devolatilization of coal/biomass blends.

Table 1. Proximate and Ultimate Analyses of Coal and Wood Samples

sample	proximate analysis			ultimate analysis				
	volatile matters (wt %, db[a])	ash (wt %, db)	fixed carbon (wt %, db)	C (wt %, db)	H (wt %, db)	O[b] (wt %, db)	N (wt %, db)	S (wt %, db)
coal	34.0	4.1	61.9	77.79	4.98	11.74	1.17	0.27
poplar wood	79.3	2.4	18.3	49.21	5.78	42.33	0.24	0.04

[a]db, dry basis. [b]Calculated by difference.

2. METHODOLOGY

2.1. Fuels. A high volatile bituminous coal was selected to be blended with a woody biomass (i.e., poplar wood). For simplicity, these feedstocks will be referred to as 'coal' and 'wood' herein. Their proximate and ultimate analyses are provided in Table 1.

Each fuel was ground in an industrial grinder similar to the one used in refs 32,34−36 and then sieved into a size fraction of 40−63 μm as in ref 32 . Wood was then blended with coal at mass fractions of 10 and 20% to obtain samples referred to as 'coal + 10% wood' and 'coal + 20% wood', respectively. These blending ratios were notably selected to evaluate the minimum amount of biomass required to initiate synergies between the blended fuels. In doing so, this work contributes to fill a gap identified when reviewing past studies undertaken to evidence synergistic effects, as most of the works were conducted using biomass contents exceeding 25 wt % (see refs 9,34 and references therein) despite the issues that could arise from the use of high mixing ratios in terms of biomass supply limitations and retrofitting costs of coal-based industrial scale boilers, for instance. All samples were dried in an oven with a constant temperature of 378 K for at least 24 h to remove excess moisture content. Samples were then stored in a desiccator to prevent moisture absorption from the atmosphere before being analyzed with the experimental facilities described in Section 2.2.

2.2. Experiments. *2.2.1. Thermogravimetric Analyzer.* Low heating rate measurements were performed at atmospheric pressure by means of a SETARAM SETSYS Evolution thermogravimetric analyzer as in refs 34,37,38. 10 mg of samples was placed into alumina crucibles before being submitted to dynamic runs at three different HRs (i.e., 10, 15, and 30 K min⁻¹). A constant 100 mL min⁻¹ flow of nitrogen was set during all of the experiments to eliminate air and continuously ensure an inert environment. Samples were heated from room temperature up to 378 K to ensure the complete removal of free water. The temperature was then continuously increased at rates of 10, 15, or 30 K min⁻¹ before plateauing at 1223 K. Three tests were performed for each fuel and each operating condition to obtain averaged profiles and hence mitigate possible slight deviations from test to test due to uncertainties and measurement noise. Mean uncertainties of ±0.63, ±0.75, ±0.65, and ±0.73% were then estimated based on a 95% confidence level for the coal, wood, coal + 10% wood, and coal + 20% wood samples, respectively.

2.2.2. Flat Flame Reactor. High heating rate measurements were carried out in a flat flame reactor previously used to study coal devolatilization and oxidation under various atmospheres.[32,35,36,39,40] This facility will only be briefly presented herein since it has already been fully described and characterized by both experimental and CFD approaches in ref 39, where diagrams of the whole experimental arrangement can be found. It consists of an atmospheric Holthuis flat flame burner composed of a 60 mm diameter bronze porous plate on

which three stoichiometric premixed propane−air flat flames (FF1, FF2, and FF3) were stabilized. These latter were produced by premixing 0.65 (FF1), 0.94 (FF2), and 1.26 (FF3) L min⁻¹ of propane with 15.4, 22.4, and 30 L min⁻¹ of air, respectively.[32] This resulted in different heating conditions being generated. For pulverized fuels (i.e., coal, wood, and their blends), they were introduced into an acoustic sower with a mass flow rate of 12 g h⁻¹. They were then fluidized by a 1 L min⁻¹ nitrogen flow to be pneumatically transported to a 1.5 mm internal diameter injector placed at the center of the burner. This experimental arrangement enables heating the fuel particles driven by the central nitrogen flow with an HR of ∼10⁶ K s⁻¹.[32,39] As such, the tested fuels rapidly devolatilize in an oxygen-deprived environment, as verified through measurements and CFD calculations.[39] The FFR is, moreover, isolated from the external environment by means of a 40 cm high quartz chimney sheltered by an insulation cover with optical accesses built in for optical measurements. Partially devolatilized fuel particles were sampled at different heights above the burner (i.e., at different residence times) by means of a 51 cm high quartz collector equipped with nitrogen injectors, ensuring an immediate quenching of the samples.[40] Particles were driven to a heated cyclone (Dekati SAC-65) to be recovered. They were then analyzed to derive devolatilization rates using the ash tracer, following the procedure described in refs 33 and 41 . To that end, 50 μm silica particles were heated at 1073 K in a muffle furnace for 4 h before being mixed with the studied fuels with a 0.1/0.9 mass ratio (see ref 41 for more details on this procedure). Finally, the thermal history of the fuel particles was systematically characterized by particle image velocimetry and two-color infrared pyrometry measurements.[32,39] This especially led to the estimation of peak fuel temperatures of ∼1020, ∼ 1109, and ∼1206 K for FF1, FF2, and FF3, respectively. Three samples were collected for each measurement point (as was the case for TGA measurements) in order to obtain the averaged results reported in Section 3. Mean uncertainties of ±3.63, ±5.89, ±4.54, and ±3.28% were thus estimated based on a 95% confidence level for the coal, wood, coal + 10% wood, and coal + 20% wood samples, respectively. Although being greater than the uncertainties related to the TGA measurements, such values remain consistent with the errors commonly reported in DTF experiments[29] as well as with the uncertainty ranges reported in previous studies conducted with the same FFR.[32,35,36]

2.3. Kinetic Modeling and Optimization Procedure. *2.3.1. CPD Model.* The CPD model was proposed by Grant et al.[22,42,43] to simulate the devolatilization behavior of coal. It is based on the percolation theory and uses a lattice model to account for the fuel chemical structure which is represented as a polymer-like network of fused aromatic clusters connected by nonaromatic chemical bridges. During the devolatilization process, labile bridges become unstable as a result of fuel heating and may undergo breakage following a reaction sequence depicted as follows:

Table 2. Rate Coefficients and Fuel Structural Parameters Used in the CPD Model

rate coefficients	coal[22]	cellulose[45]	hemicellulose[45]	lignin[45]
E_b (kcal mol^{-1})—bridge scission activation energy	55.4	55.4	51.5	55.4
A_b (s^{-1})—bridge scission pre-exponential factor	2.6×10^{15}	2.0×10^{16}	1.2×10^{20}	7.0×10^{16}
σ_b (kcal mol^{-1})—bridge scission standard deviation	1.8	4.1	0.1	0.5
E_g (kcal mol^{-1})—gas release activation energy	69.0	61.2	38.2	69.0
A_g (s^{-1})—gas release pre-exponential factor	3.0×10^{15}	3.0×10^{15}	3.0×10^{15}	2.3×10^{19}
σ_g (kcal mol^{-1})—gas release standard deviation	8.1	8.1	5.0	2.6
k_δ/k_c – composite rate constant	0.9	100	1.35	1.7
E_{cross} (kcal mol^{-1})—cross-linking activation energy	65.0	65.0	65.0	65.0
A_{cross} (s^{-1})—cross-linking pre-exponential factor	3.0×10^{15}	3.0×10^{15}	3.0×10^{15}	3.0×10^{15}
structural parameters	**coal**	**cellulose[45]**	**hemicellulose[45]**	**lignin[45]**
$M_{cluster}$—average molecular weight per cluster	266.6[a]	81	77.5	208
M_δ—average molecular weight per side chain	27.4[a]	22.7	21.5	39
p_0—initial fraction of intact bridges between clusters	0.594[a]	1.0	1.0	0.71
$\sigma + 1$—coordination number	4.83[a]	3.0	3.0	3.5
c_0—initial fraction of stable bridges	0.0[a]	0.0	0.0	0.0

[a]Calculated based on the correlations from Genetti et al.[44] using the results of the proximate and ultimate analyses reported in Table 1.
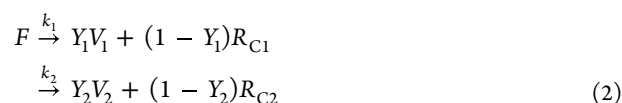
$$\pounds \xrightarrow{k_b} \pounds^* \begin{cases} \xrightarrow{k_\delta} 2\delta \xrightarrow{k_g} 2g_1 \\ \\ \xrightarrow{k_c} c + 2g_2 \end{cases}$$

(1)

where £ is a labile bridge, £* represents a reactive bridge intermediate, δ is a side chain, c stands for a char bridge, and g_1 and g_2 denote light gases, while k_b, k_δ, k_g, and k_c stand for the Arrhenius-type rate constants of the different reactions reported in eq 1. The bridge-breaking process thus begins with the decomposition of a labile bridge £ to form an activated complex £* which rapidly reacts to generate either a side chain δ or char c and gas g_2. The so-formed side chain can eventually undergo a cracking process to be converted into light gases g_1. To estimate the quantity of gaseous species emitted during the devolatilization process, the CPD model requires setting the values of five input parameters, including the number of attachments per cluster (also called the coordination number ($\sigma + 1$)), the initial fraction of intact bridges between clusters (p_0), the initial fraction of stable bridges (c_0), and the average molecular weights of aromatic clusters ($M_{cluster}$) and side chains (M_δ). These structural parameters can be experimentally assessed through ^{13}C nuclear magnetic resonance (NMR) measurements and data fitting or by using correlations based on the fuel ultimate and proximate analyses,[44] as was done in the present work. As for the rate coefficients (see Table 2), their values were proposed by Grant et al.[22] to account for the high HR pyrolysis of coal.

As mentioned in Section 1, the CPD model was also extended by Fletcher et al. to apply to biomass.[25] To that end, separate rate coefficients and structural parameters were proposed for the three main biopolymers comprising woody biomass (i.e., cellulose, hemicellulose, and lignin), as shown in Table 2. One calculation is thus operated for each of these components, considering similar operating conditions (i.e., identical thermal histories). The devolatilized fraction of the whole biomass can then be computed by merging the results of the three calculations on the basis of the mass percent of each component comprising the studied feedstock.

As for the calculation procedure, the code proposed by Perry et al.[46,47] was used as in our previous studies focusing on coal devolatilization and oxidation.[32,40] As mentioned above, the structural parameters for coal were calculated based on the

correlations proposed by Genetti et al.,[44] while for the wood components, they were obtained from the work of Lewis and Fletcher.[45] The mass percentages of each biopolymer comprising the poplar wood were estimated by averaging 27 lignocellulosic compositions provided in a series of works[48−53] focusing on such a feedstock (i.e., 23.24 wt % hemicellulose, 51.02 wt % cellulose, and 25.73 wt % lignin). Finally, the mass loss profiles related to blended samples were calculated based on the weighted sum of the devolatilization curves obtained for coal and wood.

2.3.2. Two-Competing Rate Model. The global kinetic model implemented in this work consists of two competitive parallel reactions[19,54] (see eq 2) occurring at low and high temperatures, respectively:

$$F \xrightarrow{k_1} Y_1 V_1 + (1 - Y_1) R_{C1}$$
$$\xrightarrow{k_2} Y_2 V_2 + (1 - Y_2) R_{C2}$$

(2)

where F denotes the fuel, V_1 and V_2 represent the volatile matters resulting from the first and second reactions, respectively, R_{C1} and R_{C2} stand for the residual char issued from both devolatilization steps, while Y_1 and Y_2 are mass stoichiometric coefficients. As for k_1 and k_2, they denote the rate constants which follow an Arrhenius equation of type:

$$k_i = A_i \times \exp\left(- \frac{E_{a,i}}{R \times T}\right)$$

(3)

in which the subscript i stands for either 1 or 2, A_i is the pre-exponential factor (s^{-1}), $E_{a,i}$ is the activation energy (J mol^{-1}), R is the universal gas constant (J mol^{-1} K^{-1}), and T stands for the temperature (K). Regarding the evolution of the fuel conversion fraction (α_F) and sample mass fraction (y_s) as a function of time (t), they are expressed following eqs 4 and 5 (see ref 55)

$$\frac{d\alpha_F}{dt} = (k_1 + k_2) \times f_{(\alpha_F)}$$

(4)

$$\frac{dy_s}{dt} = - (Y_1 k_1 + Y_2 k_2) \times f_{(\alpha_F)}$$

(5)

where $f_{(\alpha_F)}$ is the differential reaction model. The use of a simple first-order reaction model (i.e., $f_{(\alpha_F)} = 1 - \alpha_F$) has often

been considered suitable for simulating data collected for a narrow range of operating conditions. Authier et al.,[29] however, demonstrated in a detailed kinetic modeling study that this type of basic formulation was not adapted to reproducing devolatilization profiles measured through both TGA and DTF analyses. The authors, therefore, proposed a refined differential reaction model integrating an empirical fitting factor n (see eq 6) to improve the quality of curve fitting. This formulation of $f_{(\alpha_F)}$ was therefore selected herein to allow predicting data measured with heating rates extending from a few tens of Kelvin per minute up to $\sim10^6$ K s^{-1}.

$$f_{(\alpha_F)} = (1 - \alpha_F)^{1 + n \times \alpha_F^2} \tag{6}$$

2.3.3. Model Parametrization and Resolution Approach. Parametrizing the above-described two-step devolatilization model fundamentally requires defining seven parameters, including two couples of Arrhenius parameters (i.e., A_i and $E_{a,i}$), two stoichiometric coefficients Y_i, in addition to the reaction order factor n. To this end, one can first test different sets of parameters proposed in the literature, as will be realized in Section 3.2.1. Since these parameters are, however, derived from experiments conducted with different fuels and under widely varying operating conditions, their use often leads to unsatisfactory results.[32] Consequently, one can alternatively parametrize global kinetic models through an optimization procedure, allowing to estimate the values that A_i, $E_{a,i}$, Y_i, and n must take in order to obtain the best fit between measured and simulated data. This second approach, whose application will be shown in Section 3.2.2, aims to minimize a standard least-squares objective function (lsq) based on the relative difference between measured (y_s^{exp}) and simulated (y_s^{num}) sample mass fractions (see refs 29, 32, and 55 for instance):

$$\text{lsq} = \sum_i \frac{1}{N_i} \times \sum_j \left[\frac{\left(1 - y_s^{exp}\right) - \left(1 - y_s^{num}\right)}{\left(1 - y_s^{exp}\right)} \right]^2 \tag{7}$$

where i denotes a series of TGA and FFR runs, N_i stands for the number of experimental runs for each series, and j represents the number of discretized and equally spaced points used to calculate the least-squares difference for each series. As far as the numerical setup is concerned, the differential equations eqs 4 and 5 were solved using the MATLAB ode15s function. The solutions obtained were then integrated into a genetic algorithm-based optimizer (i.e., the MATLAB ga solver previously used to parametrize refined laser-induced incandescence models[56−59]), which allowed to define the parameter values minimizing the lsq objective function. Following Authier et al.,[29] lower and upper boundaries (listed in Table 3) were set to downsize the research area. Finally, and due to the high

number of unknown parameters, a population size of 5000 individuals and a maximum of 150 generations were set for the calculations. This proved to be sufficient, since less than 132 generations were ultimately required for optimization convergence.

3. RESULTS AND DISCUSSION

3.1. Comparison of Measured Data with Predictions Issued from the CPD Model. Following the formalism adopted in ref 29, we plotted devolatilization profiles measured during both TGA and FFR experiments in Figure 1, together with the predictions issued from the CPD model. This network simulation tool was tested as a first step, as it considers the detailed structure of thermally treated fuels (see Sections 1 and 2.3.1). It is thus more likely to properly mimic the general devolatilization behavior of a wide variety of feedstocks as compared to global models integrating non-fitted kinetic parameters. Besides, and since one of the main objectives of this work is to rule on the ability of a parametrized two-step kinetic scheme to lead to predictions at least as good as those issued from a more comprehensive phenomenological model, weighing the predictive ability of the CPD model was thus a must.

Looking at the experimental results reported in Figure 1, it can first be seen that the higher the peak fuel temperature, the higher the final devolatilized fraction during the FFR experiments. This is clearly exemplified by the mass losses for which the devolatilization profiles plateau, which increase when passing from FF1 to FF3, regardless of the considered fuel. The final devolatilized fractions assessed with the FFR are, moreover, higher than those issued from the proximate and thermogravimetric analyses despite the lower temperatures reached during FFR experiments (between 1020 and 1206 K for FF1 and FF3, respectively (see Section 2.2.2) against 1223 K during the TGA tests (see Section 2.2.1)). The ratios between the maximum volatile matter yields derived from the FFR experiments and the proximate volatile matter contents are thus ~1.2 and ~1.3 on a dry ash-free basis for wood and coal, respectively. This trend is actually in line with the observations from numerous works covering the devolatilization of solid fuels such as coal under high HR conditions.[19,20,29,32,54,55] In fact, the rapid formation of most volatiles during high HR devolatilization occurs after the fuel has reached high temperatures. As a consequence, more hydrogenation and stabilization of reactive species are likely to occur through the interchange of hydrogen atoms among the volatiles inside the fuel particles. This in turn may reduce polymerization and char formation, thus explaining the higher volatile matter yields observed during FFR measurements. As such, obtained results clearly show why slow TGA-derived kinetic data are intrinsically unsuitable for simulating measurements performed under fast thermal conditions, as explained in Section 1. This, moreover, illustrates the importance of coupling analyses conducted at low and high HR to derive kinetic parameters valid over an extended range of thermal conditions, as proposed hereafter. To conclude, it is noteworthy that in accordance with the results of the proximate analyses (see Table 1), devolatilized fractions measured for wood are much higher than those related to coal (see Figure 1). Peak mass loss fractions of 0.81 and 0.94 are indeed assessed for the biomass under TGA and FFR conditions, respectively, versus values of 0.35 and 0.47 for coal. As for blended samples, measured mass loss fractions quite logically
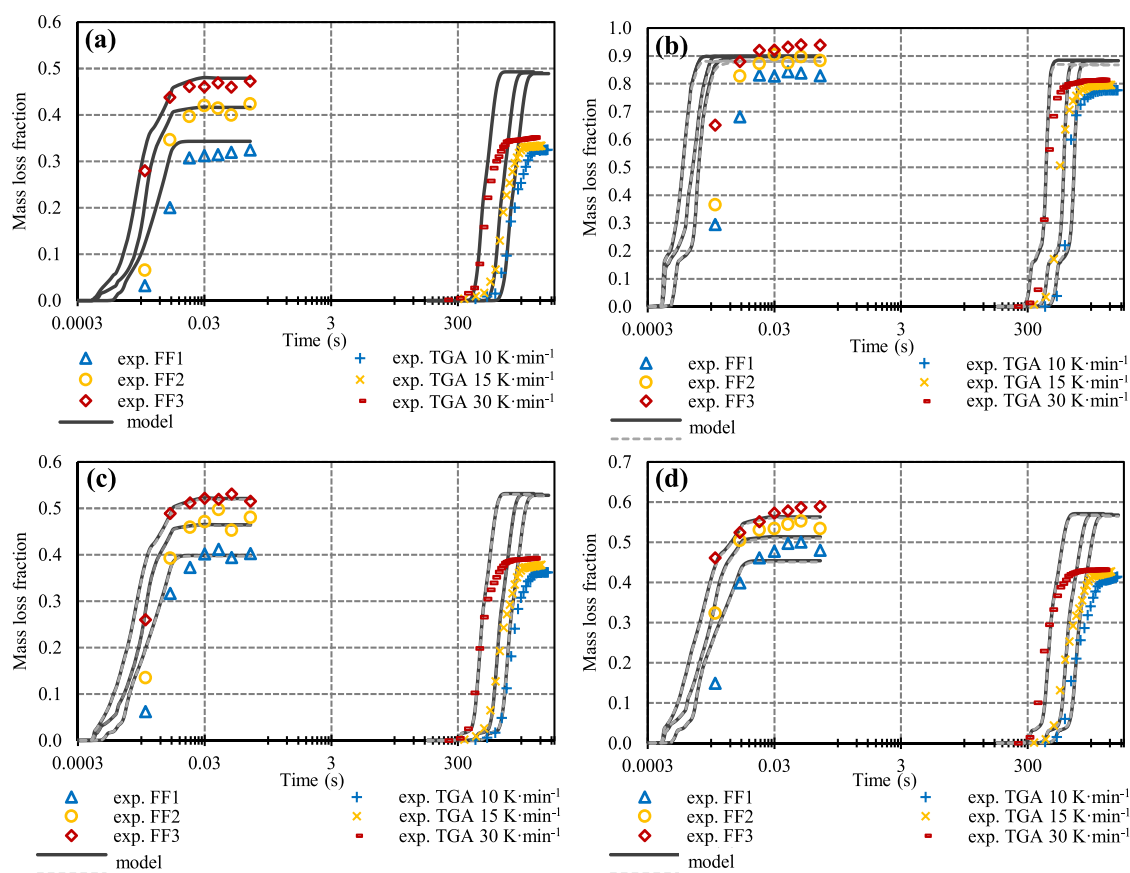
Table 3. Constraints Set during the Optimization Procedure (With A Expressed in s^{-1} and E_a in kJ mol^{-1})

parameter	lower boundary	upper boundary
$\ln(A_1)$	4.6	13.85
E_{a1}	60×10^3	120×10^3
$\ln(A_2)$	11.5	27.63
E_{a2}	120×10^3	230×10^3
y_1	0	y_2
y_2	y_1	1
n	2	12

Figure 1. Mass loss fractions of (a) coal, (b) wood, (c) coal + 10% wood, and (d) coal + 20% wood as a function of time. Comparison of measured profiles (symbols) with predictions issued from the CPD model (lines). Note that only a limited number of points are represented on each TGA curve to avoid overloading the graphs.

fall between those of wood and coal (i.e., from 0.39 to 0.43 for the blends containing 10 and 20 wt % of wood under low HR conditions versus 0.52 to 0.59 during high HR measurements). It should, however, be noted that such results do not allow evidencing any synergy at this stage. Ruling on this specific aspect will indeed require a more precise analysis of the kinetic parameters accounting for the devolatilization behavior of each sample, as proposed in Section 3.3.

Concerning CPD simulations, the procedure described in Section 2.3.1 was applied to obtain the theoretical profiles plotted with the full lines in Figure 1. As can be seen, the model globally reproduces well the devolatilization profiles issued from the FFR experiments for the three coal-containing samples (see Figure 1a,c,d). In addition to qualitatively capturing the overall shape of the devolatilization curves, the maximum volatile matter yields predicted by the model only differ from their experimental counterparts by 2.9% on average (3.0% for coal, 1.1% for coal + 10% wood, and 4.7% for coal + 20% wood). On the other hand, the model tends to significantly overpredict the rate of emission of volatile matters in the case of wood (see Figure 1b) although it reproduces relatively well the final mass loss fractions with a mean relative deviation of 3.8%. As far as the TGA results are concerned, the CPD model fails to properly simulate the measured data. It indeed overestimates the devolatilization yields, especially for coal-containing samples. The final mass loss fractions are indeed overpredicted by 45.3, 40.3, and 33.7% (on average, considering the three HR) for the coal, coal + 10% wood, and coal + 20% wood samples, respectively, against 11.2% for the

wood sample whose devolatilization behavior at low HR is much more effectively predicted. For completeness, additional CPD calculations were performed by differentiating between the contributions of xylan and glucomannan, as initially proposed by Fletcher et al.[25] To that end, the mass percentages of both these polysaccharides in poplar wood were assessed by averaging some lignocellulosic compositions available in the literature.[48,49] The rate coefficients and structural parameters proposed by Fletcher et al.[25] were then selected to be integrated within the CPD code. Despite a slightly improved agreement between experimental and simulated data for wood (see the final devolatilized fractions measured by TGA in Figure 1b), the obtained profiles, plotted with gray dashed lines, are almost superimposed with the devolatilization curves issued from the use of the parameters proposed by Lewis and Fletcher[45] for hemicellulose. Such a refinement of the calculation procedure does not thus allow reducing the abovementioned discrepancies between the measured and modeled profiles.

To conclude, it is noteworthy that the overall ability of the CPD model to reproduce mass loss profiles issued from high HR measurements is consistent with the conclusions drawn in different works,[45,60] including a previous FFR-based study in which the devolatilization of seven coals was satisfactorily simulated by the CPD model.[32] Similarly, the fact that this modeling tool tends to overestimate the total volatile yields measured during the low HR pyrolysis of biomass was previously reported by Hameed et al.[14] In an attempt to ensure that the overestimation observed during low HR

measurements was not specific to the experimental data gathered herein, we performed complementary simulations to reproduce the TGA results issued from a series of kinetic works conducted with a wide variety of coal, biomass, and biomass components.[61−68] The so-obtained correlation between the measured and predicted devolatilized fractions is depicted in Figure 2. As can be seen, the modeled data quite
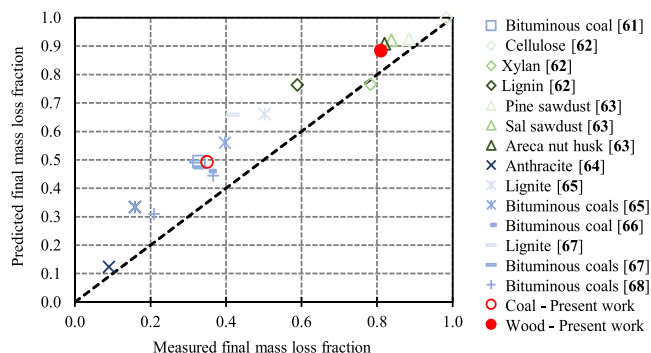

Figure 2. Correlation between the final mass loss fractions measured by TGA in refs 61−68 and those predicted herein using the CPD model.

systematically overpredict the experimentally assessed ones, which is consistent with the observation made herein. This is particularly highlighted in Figure 2 by the fact that all plotted points, except one, are located above the identity line, which is represented by a dashed line. It can also be noted that the points related to the coal and wood samples analyzed in this work clearly fall within the point cloud reported in Figure 2. This therefore tends to corroborate the relative inability of the CPD model to satisfactorily simulate the data obtained at very low heating rates. This observation especially motivated the realization of additional works aimed at improving the predictive ability of the CPD code by defining kinetic parameters adapted to account for the devolatilization of solid fuels under low HR conditions (see ref 27 and references therein). These alternative model formulations were, however, not considered, as they fall outside of the scope of the present work, which covers the prediction of the devolatilization behavior of coal and wood over an extended range of thermal conditions.

3.2. Comparison of Measured Data with Predictions Issued from a Two-Competing Rate Model. *3.2.1. Simulations Based on Kinetic Parameters from the Literature.* As mentioned in Section 2.3.3, kinetic parameters issued from the literature (see Table 4) were tested as a first step in order to rule on their suitability to simulate the mass loss profiles reported in this work. To this end, values of pre-exponential factors and activation energies proposed by Authier et al.[29] (sets 1 and 2) and Ubhayakar et al.[54] (set 3) were considered.

These data were selected since they are issued from analyses conducted with fuels having properties relatively similar to those of the bituminous coal studied herein. Regarding poplar wood, kinetic parameters proposed in the literature for two-step kinetic schemes are quite rare (if at all existing), to the best of the authors' knowledge. Kinetic factors proposed by Li et al.[69] (originally fitted to simulate the high-temperature and rapid devolatilization of palm kernel shell) were therefore considered (set 4) due to the lack of more adapted parameters.

Using the calculation procedure described in Section 2.3.2, the theoretical devolatilization profiles plotted in Figure 3 were obtained. As can be seen, none of the tested parameter sets allow to reproduce the measured data. The mass loss fractions issued from FFR experiments are indeed significantly underestimated, regardless of the sets of A_i, $E_{a,i}$, Y_i, and n values integrated in the model. As for the simulation of the devolatilization process at low HR, the two-competing rate scheme overpromotes the reactions occurring at low temperatures, thus leading to computed profiles reaching the final mass losses too early. That being said, and despite these discrepancies, it can still be noted that the parameters proposed by Ubhayakar et al.[54] (set 3) are those that provide the best agreement with FFR measurements, which is in line with the observations made in a previous work.[32] Concerning the parameter sets 1 and 2, they allow one to obtain a relatively good fit with TGA results although they fail to reproduce the data collected using the FFR. Finally, the use of parameter set 4 is shown to be clearly unsuitable for simulating the devolatilization of poplar wood under both low and high HR conditions. While this result may have been expected (the kinetic factors from Li et al.[69] being indeed optimized for another type of biomass), it is noteworthy that parameter sets 1−3 also fail to properly reproduce the experimental results collected herein, notwithstanding the use of a relatively similar fuel than those analyzed in the studies of Authier et al.[29] and Ubhayakar et al.[54] Different factors are essentially prone to influencing the validity domain of kinetic parameters derived from experimental measurements. These include a wide variability in existing fuels whose physical−chemical properties vary significantly (even within the same rank for coal). Furthermore, the measurement and calculation procedures implemented to derive the rate constants are also likely to drastically influence the results obtained. As an example, parameter sets 1 and 2 are issued from measurements conducted in a DTF with a maximum HR of the order of 4 × 10⁴ K s⁻¹, which is lower than the HR related to the FFR used in the present work. Furthermore, the thermal histories of the fuel particles during the DTF experiments from Authier et al.[29] were assessed by solving an energy balance equation, whereas they were directly measured herein. Although these differences do not challenge the consistency of the very rigorous work carried out by Authier et al.,[29] these are some

Table 4. Kinetic Parameters Proposed in the Literature to Simulate the Devolatilization of Coal and Biomass by Means of Two-Competing Rate Models

parameter set	A_1 (s⁻¹)	$E_{a,1}$ (kJ mol⁻¹)	Y_1	A_2 (s⁻¹)	$E_{a,2}$ (kJ mol⁻¹)	Y_2	n
set 1—coal[29]	1.50×10^{03}	79.7	$VM_0{}^a$	1.60×10^{08}	170.5	0.61	3.3
set 2—coal[29]	8.10×10^{05}	116.2	$VM_0{}^a$	3.00×10^{11}	221.1	0.63	5.3
set 3—coal[54]	3.70×10^{05}	73.6	$VM_0{}^a$	1.46×10^{13}	251.0	0.80	0
set 4—biomass[69]	6.20×10^{02}	42.5	0.86	8.00×10^{04}	130.0	0.96	0

^{a}VM₀, volatile matter content of the fuel issued from the proximate analysis (on dry and ash-free basis).
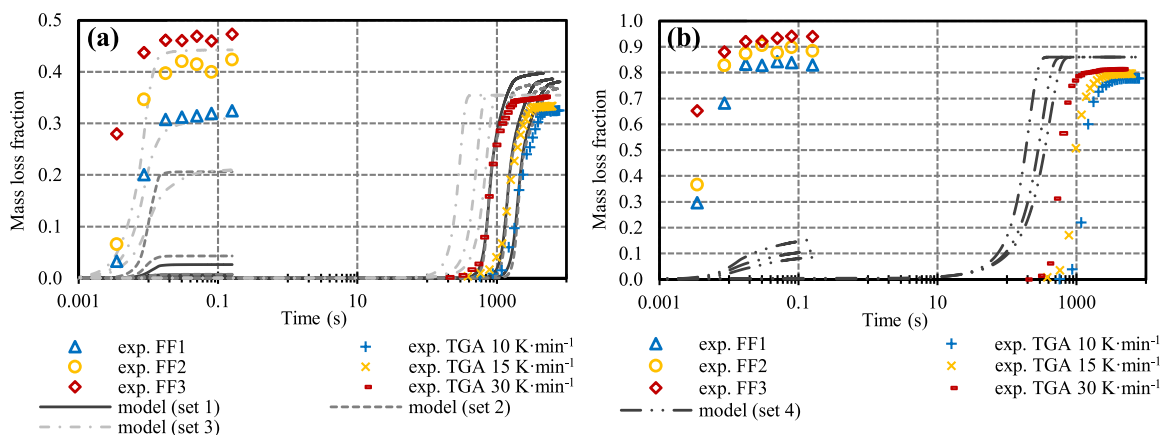
Figure 3. Mass loss fractions of (a) coal and (b) wood as a function of time. Comparison of measured (symbols) and simulated (lines) profiles integrating the kinetic parameters reported in Table 4.

Table 5. Optimized Kinetic Parameters Derived for the Two-Competing Rate Model

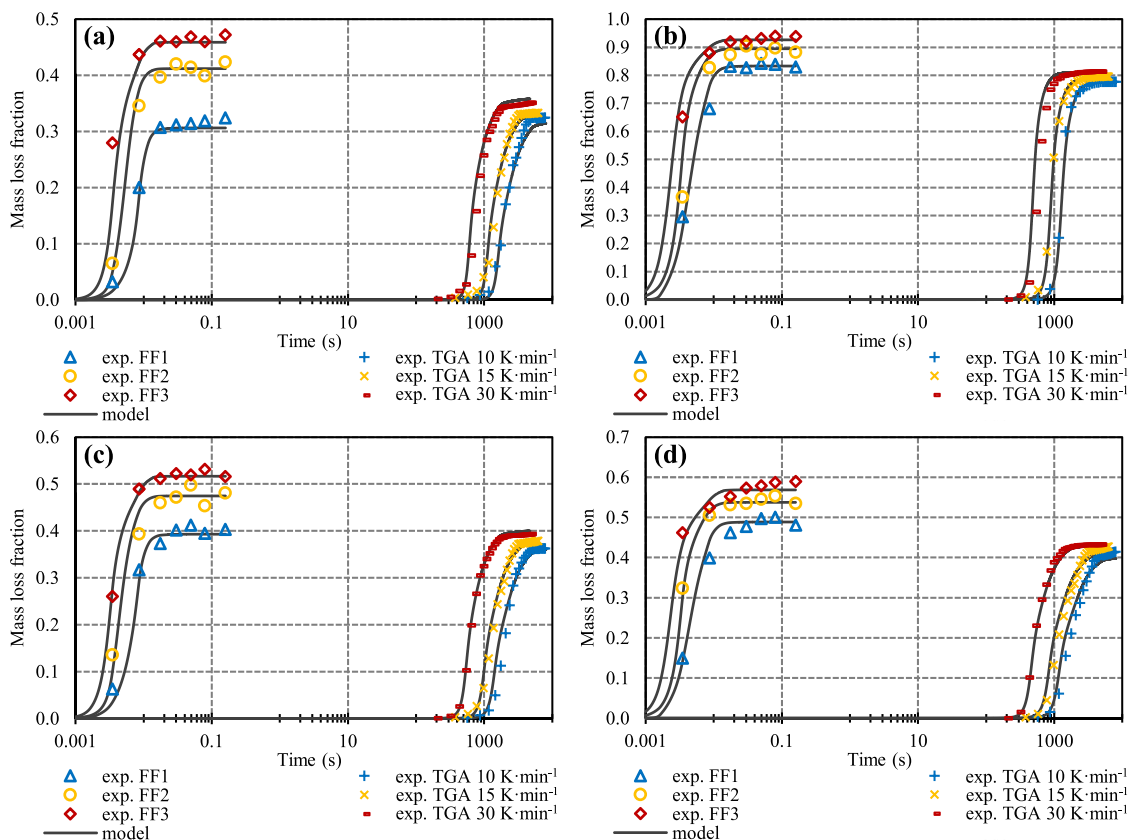| sample	A_1 (s^{-1})	$E_{a,1}$ (kJ mol^{-1})	Y_1	A_2 (s^{-1})	$E_{a,2}$ (kJ·mol^{-1})	Y_2	n
coal	2.94×10^{03}	99.79	0.162	6.56×10^{11}	186.72	0.609	6.5
wood	3.91×10^{05}	91.29	0.677	4.22×10^{11}	164.89	0.972	2.2
coal +10% wood	7.86×10^{04}	87.94	0.239	4.98×10^{11}	179.21	0.665	5.9
coal +20% wood	1.89×10^{05}	86.10	0.299	7.82×10^{11}	171.57	0.685	5.7

Figure 4. Mass loss fractions of (a) coal, (b) wood, (c) coal + 10% wood, and (d) coal + 20% wood as a function of time. Comparison of measured (symbols) and simulated (lines) profiles integrating the optimized kinetic parameters reported in Table 5.

factors which can explain why the parameters listed in Table 4 did not allow to satisfactorily simulate the devolatilization profiles measured herein. This therefore prompts the need for alternative model parametrizations, as proposed in Section 3.2.2.

3.2.2. Simulations Based on Optimized Kinetic Parameters. The implementation of the optimization procedure described in Section 2.3.3 led to inferring the kinetic parameters summarized in Table 5. The simulated devolatilization profiles obtained by using the parameters are plotted in

Figure 4, together with their experimental counterparts. As can be seen, modeled data qualitatively and quantitatively agree with measured ones. In addition to faithfully reproducing the overall shape of the devolatilization curves, the mean relative deviation between predicted and measured final mass losses falls below 1.70%, considering both TGA and FFR analyses (with values ranging from 0.87% for wood to 2.8% for coal). The good ability of the parametrized model to reproduce measured data is further illustrated in Figure 5, which depicts
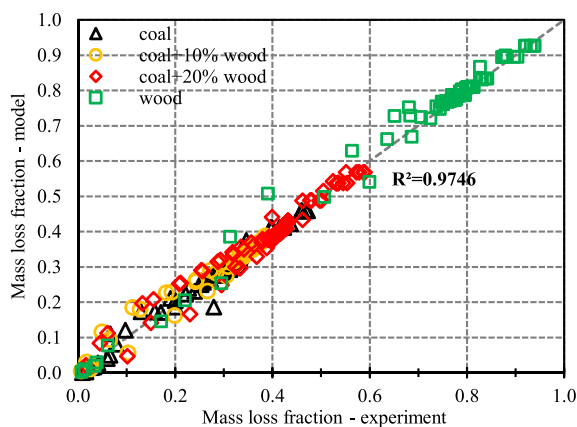

Figure 5. Correlation between measured and predicted devolatilized fractions.

the correlation existing between the calculated and measured mass losses for each point comprising the profiles plotted in Figure 4. It is then of interest to note that the obtained coefficient of determination, which denotes the dispersion of data around the identity line (represented by a dotted line), is very high ($R^2 = 0.9746$). This therefore illustrates the excellent agreement obtained between simulated and measured results (all points being indeed almost superimposed on the identity line). In an attempt to potentially refine the solution obtained, additional calculations based on a generalized reduced gradient solver (used in a previous work[32]) were carried out. For that, intervals of ±20% around the optimized values listed in Table 5 were set (except for y_2, whose upper bound was set to 1 in the case of wood). Doing so, however, did not allow the reduction of the values of the least-squares objective function defined in eq 7. This complementary validation therefore demonstrates that the optimization procedure proposed in Section 2.3.3 is adequate to infer kinetic parameters suitable to account for the devolatilization of different feedstocks over a large range of thermal conditions.

Looking at the rate constant parameters listed in Table 5, it can first be noted that in accordance with the results of the proximate analyses and with the feedstock mixing ratios set for blended samples, the values of the stoichiometric coefficients y_1 and y_2 follow the sequence: coal < coal + 10% wood < coal + 20% wood < wood. This trend is actually in line with the increasing devolatilized fractions experimentally monitored when passing from coal to wood (see Section 3.1 as well as Figure 1 or 4). Furthermore, it is noteworthy that the $E_{a,i}$ values inferred for wood are lower than those related to coal, which, here again, is consistent with the higher energy required to break the strong C−C bonds which hold the highly cross-linked aromatic structures of coal, as compared to the inter- and intra-molecular links in biomass, which break more easily under heating. It can further be noted that the values of the

empirical reaction model factor n estimated herein (i.e., between 2.2 and 6.5) are globally in line with the range of values estimated by Authier et al. (i.e., between 3.3 and 5.3) in their study on the devolatilization of three different coals.[29] All of these observations thus contribute to corroborate the consistency of the kinetic parameters assessed in the present work, whose values are physically valid, while agreeing with the data issued from other studies.

3.3. Analysis of Synergistic Effects. When analyzing in more detail the parameters gathered in Table 5, it can be seen that the activation energy of the first devolatilization reaction decreases when adding wood to coal. It indeed passes from 99.79 kJ mol^{-1} for pure coal to 87.94 and 86.10 kJ mol^{-1} for coal + 10% wood and coal + 20% wood, respectively. While such a decrease is consistent with the fact that the activation energy of wood is lower than that of coal, it is noteworthy that the $E_{a,1}$ values inferred for the blends become even lower than that related to pure wood (i.e., 91.29 kJ mol^{-1}). This trend is all the more remarkable given the relatively low blending ratios (≤20 wt %) considered in the present study. All these observations, therefore, suggest the presence of synergistic effects prone to shifting the thermal degradation of the blended samples toward lower temperatures as compared to those governing the devolatilization of raw wood. Synergistic effects are indeed known to decrease the activation energy of devolatilization reactions while enhancing the yields of volatile matters and gaseous species (see refs 9 and 70 and references therein). On the other hand, it can still be noted that the $E_{a,2}$ values estimated for coal + 10% wood and coal + 20% wood (i.e., 179.21 and 171.57 kJ mol^{-1}, respectively) fall between those related to coal (186.72 kJ mol^{-1}) and wood (164.89 kJ mol^{-1}). This suggests that synergies decrease with increasing temperature, which is once again consistent with the trends reported in the literature.[9,70] It is believed that synergies are mainly traced to hydrogen donors from biomass, which prevent recombination reactions of coal radicals. When the temperature increases, the amount of hydrogen released from coal tends to increase as well, thus limiting the extent of synergistic effects. To better appreciate whether or not synergies truly act during the tests performed herein, we estimated the deviation Δy_s between the mass losses calculated for blended samples (referred to as "blend" in eq 8 below) and the weighted sum of the mass losses estimated for individual components of the blends:

$$\Delta y_s = \left(\int_t - (Y_1 k_1 + Y_2 k_2) \times f_{(\alpha_F)} \right)_{blend}$$
$$- \left[W \times \left(\int_t - (Y_1 k_1 + Y_2 k_2) \times f_{(\alpha_F)} \right)_{wood} \right.$$
$$\left. + (1 - W) \times \left(\int_t - (Y_1 k_1 + Y_2 k_2) \times f_{(\alpha_F)} \right)_{coal} \right]$$

$$(8)$$

where W denotes the mass fraction of wood in the blend. Positive deviations logically suggest that the blending of wood and coal enhances the decomposition process, thus leading to a quantity of emitted volatile matters exceeding that expected by summing the mass losses related to the individual devolatilization of both feedstocks. Using the kinetic parameters of Table 5, one obtains the curves depicted in Figure 6 for the blend containing 20% of biomass as an example. The fact that the calculated Δy_s values are positive confirms the probable
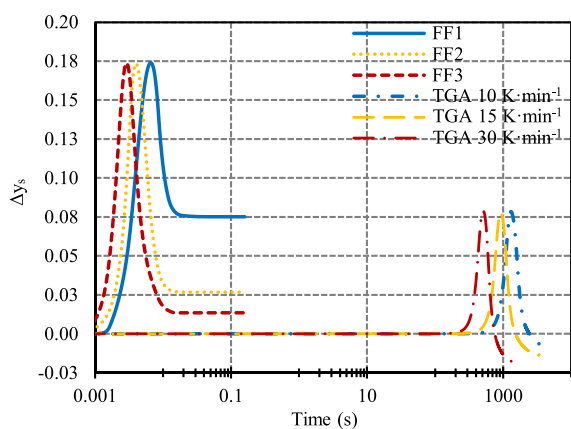
Figure 6. Evolution of Δy_s as a function of time for coal + 20% wood as a function of time.

presence of synergies. It should be noted that a similar behavior was also observed with the blend containing 10% of wood (results not reported herein for brevity). Furthermore, it is interesting to note that Δy_s values rise from low to intermediate residence times before decreasing, regardless of the experimental configurations considered (i.e., TGA and FFR). The fact that the temperatures encountered in these specific regions of the devolatilization curves are relatively low (i.e., below 650 K during TGA tests, for instance) tends to corroborate the above statement that the lower the temperature, the higher the synergies.

To further validate the conclusions drawn based on Figure 6, the evolution of the rate constants k_1 and k_2 (see eqs 4 and 5), as well as the variation of the characteristic time of devolatilization, was plotted as a function of temperature in Figure 7 a,b. As can be seen, for temperatures below ~700 K, the values of k_1 for the coal + 20% wood sample are higher than those related to wood. As a consequence, the characteristic time of devolatilization of this blend is lower than that of wood for temperatures up to ~650 K, which confirms the existence of synergies under low heating conditions. Besides, and since the higher the activation energy, the lower the rate constant, the values of k_2 quite logically follow a sequence that is the opposite of that depicted in Table 5 for $E_{a,2}$ (i.e., $k_{2,coal} < k_{2,coal+10\% wood} < k_{2,coal+20\% wood} < k_{2,wood}$, with $k_{2,coal+20\% wood}$ quite close to $k_{2,wood}$ above 900 K). Finally, it is noteworthy that the characteristic times related to the blend containing 10% of

wood (see Figure 7b) are relatively similar to those of coal at high temperatures, while they are significantly lower below 600 K, despite the low blending ratio related to this sample. All these observations, therefore, corroborate that synergies occur during the low-temperature devolatilization of coal/wood mixtures, thus enhancing the release of volatile matters. This trend is, moreover, consistent with the conclusions drawn in ref 34 where preliminary analyses achieved solely at low heating rates with similar coal/wood mixtures were carried out. These results should, however, be considered with caution, as they are issued from calculations based on the parameters listed in Table 5. Although there are good reasons to believe that these kinetic constants are consistent, as discussed above, any imprecision in the estimation of A_i and $E_{a,i}$ may have a significant effect on the conclusions drawn in this section. The present work would therefore benefit from being complemented by additional studies considering other feedstocks and mixing ratios, allowing to better elucidate the impact of synergistic effects on the devolatilization of coal/wood mixtures.

4. CONCLUSIONS

This work dealt with the analysis of the devolatilization behavior of two solid fuels of interest for co-pyrolysis and co-combustion applications (i.e., bituminous coal and poplar wood). TGA analyses conducted with HR of 10, 15, and 30 K min^{-1} were coupled with measurements performed using an FFR which allows to reach an HR of ~10^6 K s^{-1}. Experimental data collected with coal, wood, and their blends confirmed that the greater the HR, the greater the quantity of volatile matters emitted (devolatilization yields exceeding the proximate volatile matter contents being quite systematically measured during FFR experiments). Furthermore, the higher the biomass fraction in the blended samples, the higher the devolatilized fractions, in accordance with the higher volatile content of poplar wood. Two different modeling approaches were then implemented, including a network model (i.e., CPD), and a two-competing rate scheme, including a refined differential reaction model. In terms of highlights, the CPD model proved to be a very effective modeling tool to qualitatively capture the overall shape of devolatilization profiles, regardless of the considered fuel, while leading to final mass losses quite close to those experimentally assessed during high HR experiments. It, however, failed to properly predict the devolatilization yields
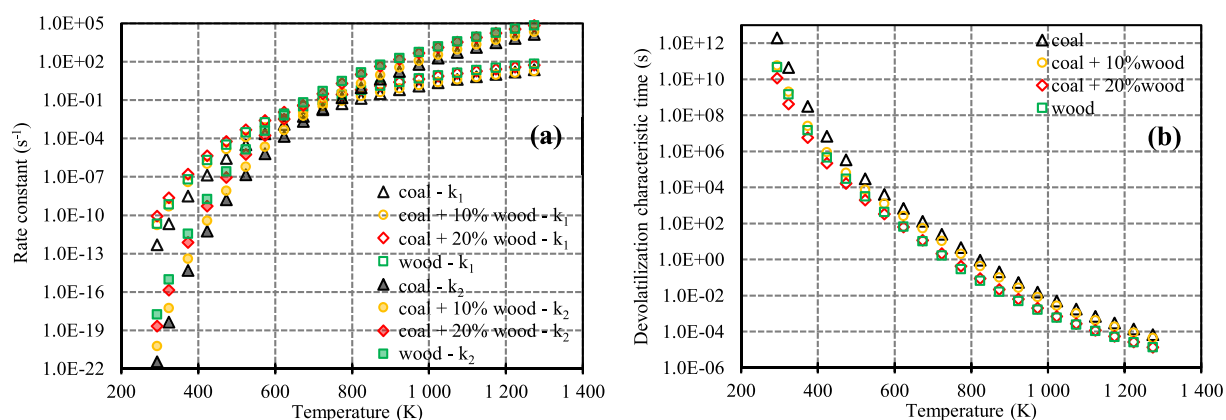

Figure 7. Variation of (a) rate constants k_1 and k_2 and (b) characteristic time of devolatilization (defined as $1/(k_1 + k_2)$) as a function of temperature.

obtained from TGA experiments. As for the two-competing rate kinetic scheme, different parameter sets from the literature were tested, providing unsatisfactory predictions. A parametrization procedure using a genetic algorithm-based optimizer was thus implemented to infer A_i, $E_{a,i}$, y_s, and n values, allowing obtaining simulated devolatilization profiles merging on a single curve with their experimental counterparts. $E_{a,i}$ values estimated for wood were found to be lower than those related to coal, which is consistent with the lower energy required to break the inter- and intra-molecular links of lignocellulosic biomass. Furthermore, the addition of wood to coal was shown to significantly decrease the activation energies of the two devolatilization reactions. The E_a value of the first reaction occurring at low temperatures was even found to be lower for blended samples than for pure wood, despite the relatively low mixing ratios considered in this work ($\leq$20 wt %). This trend was related to the existence of synergistic effects, the extent of which was demonstrated to be mainly significant for low temperatures, in agreement with the trends previously reported in the literature.

■ AUTHOR INFORMATION

Corresponding Author

Romain Lemaire − *Department of Mechanical Engineering, École de technologie supérieure, Montreal, Quebec H3C 1K3, Canada;* ⬤ orcid.org/0009-0003-5106-3925; Phone: 514 396-8727; Email: romain.lemaire@etsmtl.ca

Authors

Wei Wang − *Department of Mechanical Engineering, École de technologie supérieure, Montreal, Quebec H3C 1K3, Canada*

Sebastien Menanteau − *Energy, Environment & Materials Engineering, Icam Lille, Lille 59016, France*

Complete contact information is available at:
https://pubs.acs.org/10.1021/acsomega.3c03110

Author Contributions

Conceptualization: R.L.; methodology: R.L.; investigation and formal analysis: R.L., W.W., and S.M.; funding acquisition: R.L.; project administration: R.L.; resources: R.L.; supervision: R.L.; validation: R.L.; visualization: R.L. and S.M.; writing—original draft preparation: R.L.; writing—review and editing: R.L.

Notes

The authors declare no competing financial interest.

■ REFERENCES

(1) Finkelman, R. B.; Wolfe, A.; Hendryx, M. S. The future environmental and health impacts of coal. *Energy Geosci.* **2021**, *2*, 99−112.

(2) Yao, Z.; Reinmöller, M.; Ortuno, N.; Zhou, H.; Jin, M.; Liu, J.; Luque, R. Thermochemical conversion of waste printed circuit boards: Thermal behavior, reaction kinetics, pollutant evolution and corresponding controlling strategies. *Prog. Energy Combust. Sci.* **2023**, *97*, No. 101086.

(3) Sami, M.; Annamalai, K.; Wooldridge, M. Cofiring of coal and biomass fuel blends. *Prog. Energy Combust. Sci.* **2001**, *27*, 171−214.

(4) Demirbas, A. Sustainable cofiring of biomass with coal. *Energy Convers. Manag.* **2003**, *44*, 1465−79.

(5) Leckner, B. Co-combustion: A summary of technology. *Therm. Sci.* **2007**, *11*, 5−40, DOI: 10.2298/TSCI0704005L.

(6) Saidur, R.; Abdelaziz, E. A.; Demirbas, A.; Hossain, M. S.; Mekhilef, S. A review on biomass as a fuel for boilers. *Renew. Sustain. Energy Rev.* **2011**, *15*, 2262−89.

(7) Sahu, S. G.; Chakraborty, N.; Sarkar, P. Coal-biomass co-combustion: An overview. *Renew. Sustain. Energy Rev.* **2014**, *39*, 575−86.

(8) Gerssen-Gondelach, S.J.; Saygin, D.; Wicke, B.; Patel, M. K.; Faaij, A. P. C. Competing uses of biomass: Assessment and comparison of the performance of bio-based heat, power, fuels and materials. *Renew. Sustain. Energy Rev.* **2014**, *40*, 964−98.

(9) Wang, W.; Lemaire, R.; Bensakhria, A.; Luart, D. Review on the catalytic effects of alkali and alkaline earth metals (AAEMs) including sodium, potassium, calcium and magnesium on the pyrolysis of lignocellulosic biomass and on the co-pyrolysis of coal with biomass. *J. Anal. Appl. Pyrolysis* **2022**, *163*, No. 105479.

(10) Saxena, S. C. Devolatilization and combustion characteristics of coal particles. *Prog. Energy Combust. Sci.* **1990**, *16*, 55−94.

(11) Solomon, P. R.; Serio, M. A.; Suuberg, E. M. Coal pyrolysis: experiments, kinetic rates and mechanisms. *Prog. Energy Combust. Sci.* **1992**, *18*, 133−220.

(12) Papari, S.; Hawboldt, K. A review on the pyrolysis of woody biomass to bio-oil: Focus on kinetic models. *Renew. Sustain. Energy Rev.* **2015**, *52*, 1580−95.

(13) Wang, S.; Dai, G.; Yang, H.; Luo, Z. Lignocellulosic biomass pyrolysis mechanism: A state-of-the-art review. *Prog. Energy Combust. Sci.* **2017**, *62*, 33−86.

(14) Hameed, S.; Sharma, A.; Pareek, V.; Wu, H.; Yu, Y. A review on biomass pyrolysis models: Kinetic, network and mechanistic models. *Biomass Bioenergy* **2019**, *123*, 104−122.

(15) Mularski, J.; Pawlak-Kruczek, H.; Modlinski, N. A review of recent studies of the CFD modelling of coal gasification in entrained flow gasifiers, covering devolatilization, gas-phase reactions, surface reactions, models and kinetics. *Fuel* **2020**, *271*, No. 117620.

(16) Vikram, S.; Rosha, P.; Kumar, S. Recent modeling approaches to biomass pyrolysis: A review. *Energy Fuels* **2021**, *35*, 7406−33.

(17) Vyazovkin, S.; Burnham, A. K.; Criado, J. M.; Pérez-Maqueda, L. A.; Popescu, C.; Sbirrazzuoli, N. ICTAC Kinetics Committee recommendations for performing kinetic computations on thermal analysis data. *Thermochim. Acta* **2011**, *520*, 1−19.

(18) Badzioch, S.; Hawksley, P. G. W. Kinetics of thermal decomposition of pulverized coal particles. *Ind. Eng. Chem. Process Des. Dev.* **1970**, *9*, 521−30.

(19) Kobayashi, H.; Howard, J. B.; Sarofim, A. F. Coal devolatilization at high temperatures. *Symp. (Int.) Combust.* **1977**, *16*, 411−25.

(20) Anthony, D. B.; Howard, J. B.; Hottel, H. C.; Meissner, H. P. Rapid devolatilization of pulverized coal. *Symp. (Int.) Combust.* **1975**, *15*, 1303−17.

(21) Solomon, P. R.; Hamblen, D. G.; Carangelo, R. M.; Serio, M. A.; Deshpande, G. V. General model of coal devolatilization. *Energy Fuels* **1988**, *2*, 405−22.

(22) Grant, D. M.; Pugmire, R. J.; Fletcher, T. H.; Kerstein, A. R. Chemical model of coal devolatilization using percolation lattice statistics. *Energy Fuels.* **1989**, *3*, 175−86.

(23) Niksa, S.; Kerstein, A. R. FLASHCHAIN Theory for rapid coal devolatilization kinetics. 1. Formulation. *Energy Fuels* **1991**, *5*, 647−65.

(24) Chen, Y.; Charpenay, S.; Jensen, A.; Wojtowicz, M. A.; Serio, M. A. Modeling of biomass pyrolysis kinetics. *Symp. (Int.) Combust.* **1998**, *27*, 1327−34.

(25) Fletcher, T. H.; Pond, H. R.; Webster, J.; Wooters, J.; Baxter, L. L. Prediction of tar and light gas during pyrolysis of black liquor and biomass. *Energy Fuels* **2012**, *26*, 3381−7.

(26) Niksa, S. Predicting the rapid devolatilization of diverse forms of biomass with bio-flashchain. *Proc. Combust. Inst.* **2000**, *28*, 2727−33.

(27) Fletcher, T. H. Review of 30 years of research using the chemical percolation devolatilization model. *Energy Fuels* **2019**, *33*, 12123−53.

(28) Richards, A. P.; Fletcher, T. H. A comparison of simple global kinetic models for coal devolatilization with the CPD model. *Fuel* **2016**, *185*, 171−80.

(29) Authier, O.; Thunin, E.; Plion, P.; Porcheron, L. Global kinetic modeling of coal devolatilization in a thermogravimetric balance and drop-tube furnace. *Energy Fuels* **2015**, *29* (3), 1461–8.

(30) McLean, W. J.; Hardesty, D. R.; Pohl, J. H. Direct observations of devolatilizing pulverized coal particles in a combustion environment. *Symp. (Int.) Combust.* **1981**, *18*, 1239–48.

(31) Shaddix, C. R.; Molina, A. Particle imaging of ignition and devolatilization of pulverized coal during oxy-fuel combustion. *Proc. Combust Inst.* **2009**, *32*, 2091–8.

(32) Lemaire, R.; Menage, D.; Seers, P. Study of the high heating rate devolatilization of bituminous and subbituminous coals-Comparison of experimentally monitored devolatilization profiles with predictions issued from single rate, two-competing rate, distributed activation energy and chemical percolation devolatilization models. *J. Anal. Appl. Pyrolysis* **2017**, *123*, 255–68.

(33) Zellagui, S.; Schönnenbeck, C.; Zouaoui, N.; Brilhac, J. F.; Authier, O.; Thunin, E.; Procheron, L. Fast pyrolysis of coals under N_2 and CO_2 atmospheres. *J. Therm. Anal. Calorim.* **2018**, *133*, 1535–7.

(34) Wang, W.; Lemaire, R.; Bensakhria, A.; Luart, D. Thermogravimetric analysis and kinetic modeling of the co-pyrolysis of a bituminous coal and poplar wood. *Chin J. Chem. Eng.* **2023**, *58*, 53–68.

(35) Lemaire, R.; Menage, D.; Menanteau, S.; Harion, J. L. Experimental study and kinetic modeling of pulverized coal devolatilization under air and oxycombustion conditions at a high heating rate. *Fuel Process. Technol.* **2014**, *128*, 183–90.

(36) Lemaire, R.; Bruhier, C.; Menage, D.; Therssen, E.; Seers, P. Study of the high heating rate devolatilization of a pulverized bituminous coal under oxygen-containing atmospheres. *J. Anal. Appl. Pyrolysis* **2015**, *114*, 22–31.

(37) Wang, W.; Lemaire, R.; Bensakhria, A.; Luart, D. Thermogravimetric analysis and kinetic modeling of the AAEM-catalyzed pyrolysis of woody biomass. *Molecules* **2022**, *27*, 7662.

(38) Wang, W.; Lemaire, R.; Bensakhria, A.; Luart, D. Analysis of the catalytic effects induced by alkali and alkaline earth metals (AAEMs) on the pyrolysis of beech wood and corncob. *Catalysts* **2022**, *12*, 1505.

(39) Lemaire, R.; Menanteau, S. Development and numerical/experimental characterization of a lab-scale flat flame reactor allowing the analysis of pulverized solid fuel devolatilization and oxidation at high heating rates. *Rev. Sci. Instrum.* **2016**, *87* (1), No. 015104.

(40) Menage, D.; Lemaire, R.; Seers, P. Experimental study and chemical reactor network modeling of the high heating rate devolatilization and oxidation of pulverized bituminous coals under air, oxygen-enriched combustion(OEC) and oxy-fuel combustion (OFC). *Fuel Process. Technol.* **2018**, *177*, 179–93.

(41) Farrow, T. S.; Sun, C.; Snape, C. E. Impact of CO_2 on biomass pyrolysis, nitrogen partitioning, and char combustion in a drop tube furnace. *J. Anal. Appl. Pyrolysis* **2015**, *113*, 323–331.

(42) Fletcher, T. H.; Kerstein, A. R.; Pugmire, R. J.; Grant, D. M. Chemical percolation model for devolatilization. 2. Temperature and heating rate effects on product yields. *Energy Fuels* **1990**, *4*, 54–60.

(43) Fletcher, T. H.; Kerstein, A. R.; Pugmire, R. J.; Solum, M. S.; Grant, D. M. Chemical percolation model for devolatilization. 3. Direct use of ^{13}C NMR data to predict effects of coal type. *Energy Fuels* **1992**, *6*, 414–31.

(44) Genetti, D.; Fletcher, T. H.; Pugmire, R. J. Development and application of a correlation of ^{13}C NMR chemical structural analyses of coal based on elemental composition and volatile matter content. *Energy Fuels* **1999**, *13*, 60–8.

(45) Lewis, A. D.; Fletcher, T. H. Prediction of sawdust pyrolysis yields from a flat-flame burner using the CPD model. *Energy Fuels* **2013**, *27*, 942–53.

(46) Perry, S. T. *A global free-radical mechanism for nitrogen release during coal devolatilization based on chemical structure*; PhD thesis, Brigham Young University: Utah, United-States; 1999.

(47) Perry, S. T.; Genetti, D.; Fletcher, T. H.. CPD NLG Files, https://www.et.byu.edu/~tom/cpd/; 2013.

(48) Timell, T.E. Recent progress in the chemistry of wood hemicelluloses. *Wood Sci. Technol.* **1967**, *1*, 45–70.

(49) Patt, R.; Kordsachia, O.; Fehr, J. European hardwoods versus *eucalyptus globulus* as a raw material for pulping. *Wood Sci. Technol.* **2006**, *40*, 39–48.

(50) Guidi, W.; Tozzini, C.; Bonari, E. Estimation of chemical traits in poplar short-rotation coppice at stand level. *Biomass Bioenergy* **2009**, *33*, 1703–9.

(51) Sannigrahi, P.; Ragauskas, A. J.; Tuskan, G. A. Poplar as a feedstock for biofuels: A review of compositional characteristics. *Biofuels Bioprod. Bioref.* **2010**, *4*, 209–26.

(52) Rego, F.; Soares Dias, A. P.; Casquilho, M.; Rosa, F. C.; Rodrigues, A. Fast determination of lignocellulosic of poplar biomass by thermogravimetry. *Biomass Bioenergy* **2019**, *122*, 375–80.

(53) Rego, F.; Soares Dias, A. P.; Casquilho, M.; Rosa, F. C.; Rodrigues, A. Pyrolysis kinetics of short rotation coppice poplar biomass. *Energy* **2020**, *207*, No. 118191.

(54) Ubhayakar, S. K.; Stickler, D. B.; Von Rosenberg, C. W., Jr.; Gannon, R. E. Rapid devolatilization of pulverized coal in hot combustion gases. *Symp. (Int) Combust.* **1977**, *16*, 427–36.

(55) Authier, O.; Thunin, E.; Plion, P.; Schönnenbeck, C.; Leyssens, G.; Brilhac, J. F.; Porcheron, L. Kinetic study of pulverized coal devolatilization for boiler CFD modeling. *Fuel* **2014**, *122*, 254–60.

(56) Menanteau, S.; Lemaire, R. Analysis of the influence of the conduction sub-model formulation on the modeling of laser-induced incandescence of Diesel soot aggregates. *Entropy* **2020**, *22* (1), 21.

(57) Lemaire, R.; Menanteau, S. Modeling laser-induced incandescence of Diesel soot-Implementation of an advanced parameterization procedure applied to a refined LII model accounting for shielding effect and multiple scattering within aggregates for α_T and E(m) assessment. *Appl. Phys. B: Laser Opt.* **2021**, *127*, 138.

(58) Menanteau, S.; Lemaire, R. Parameterization of a refined model aimed at simulating laser-induced incandescence of soot using a visible excitation wavelength of 532 nm. *J. Adv. Res. Fluid Mech. Therm. Sci.* **2022**, *98*, 92–103.

(59) Lemaire, R.; Menanteau, S. Study of the wavelength dependence of the absorption function of diesel soot by LII modeling integrating the effect of multiple scattering within aggregates. *Appl. Phys. B: Laser Opt.* **2023**, *129*, 79.

(60) Wan, K.; Wang, Z.; He, Y.; Xia, J.; Zhou, Z.; Zhou, J.; et al. Experimental and modeling study of pyrolysis of coal, biomass and blended coal-biomass particles. *Fuel* **2015**, *139*, 356–64.

(61) Seo, D. K.; Park, S. S.; Kim, Y. T.; Hwang, J.; Yu, T. U. Study of coal pyrolysis by thermo-gravimetric analysis (TGA) and concentration measurements of the evolved species. *J. Anal. Appl. Pyrolysis* **2011**, *92* (1), 209–16.

(62) Yu, J.; Paterson, N.; Blamey, J.; Millan, M. Cellulose, xylan and lignin interactions during pyrolysis of lignocellulosic biomass. *Fuel* **2017**, *191*, 140–9.

(63) Mishra, R. K.; Mohanty, K. Pyrolysis kinetics and thermal behavior of waste sawdust biomass using thermogravimetric analysis. *Bioresour. Technol.* **2018**, *251*, 63–74.

(64) Gou, X.; Zhao, X.; Singh, S.; Qiao, D. Tri-pyrolysis: A thermo-kinetic characterisation of polyethylene, cornstalk, and anthracite coal using TGA-FTIR analysis. *Fuel* **2019**, *252*, 393–402.

(65) Yan, J.; Liu, M.; Feng, Z.; Bai, Z.; Shui, H.; Li, Z.; et al. Study on the pyrolysis kinetics of low-medium rank coals with distributed activation energy model. *Fuel* **2020**, *261*, No. 116359.

(66) Zhang, H.; Dou, B.; Zhang, H.; Li, J.; Ruan, C.; Wu, C. Study on non-isothermal kinetics and the influence of calcium oxide on hydrogen production during bituminous coal pyrolysis. *J. Anal. Appl. Pyrolysis* **2020**, *150*, No. 104888.

(67) Yu, J.; Guo, Q.; Ding, L.; Gong, Y.; Yu, G. Study on the effect of inherent AAEM on char structure evolution during coal pyrolysis by in-situ Raman and TG. *Fuel* **2021**, *292*, No. 120406.

(68) Niu, Z.; Liu, G.; Yin, H.; Zhou, C.; Wu, D.; Tan, F. A comparative study on thermal behavior of functional groups in coals with different ranks during low temperature pyrolysis. *J. Anal. Appl. Pyrolysis* **2021**, *158*, No. 105258.

(69) Li, J.; Bonvicini, G.; Tognotti, L.; Yang, W.; Blasiak, W. High-temperature rapid devolatilization of biomasses with varying degrees of torrefaction. *Fuel* **2014**, *122*, 261−9.

(70) Gouws, S. M.; Carrier, M.; Bunt, J. R.; Neomagus, H. W. J. P. Co-pyrolysis of coal and raw/torrefied biomass: A review on chemistry, kinetics and implementation. *Renew. Sustain. Energy Rev.* **2021**, *135*, No. 110189.